RPP-35977
Revision 0

# Impact Assessment of Existing Vadose Zone Contamination at the Hanford Site SX Tank Farm

Prepared for the U.S. Department of Energy
Assistant Secretary for Environmental Management

Contractor for the U.S. Department of Energy
Office of River Protection under Contract DE-AC27-99RL14047

CH2MHILL
*Hanford Group, Inc.*

***P.O. Box 1500***
***Richland, Washington***

RPP-35977
Revision 0

# Impact Assessment of Existing Vadose Zone Contamination at the Hanford Site SX Tank Farm

J. G. Kristofzski
Chair, American Geophysical Union
CH2M HILL Hanford Group, Inc.

R. Khaleel
Fluor Government Group

Date Published
November 2007

To Be Presented at
Vadose Zone Journal - online publication

Soil Science Society of America
November 20, 2007

Prepared for the U.S. Department of Energy
Assistant Secretary for Environmental Management

Contractor for the U.S. Department of Energy
Office of River Protection under Contract DE-AC27-99RL14047

CH2MHILL
*Hanford Group, Inc.*
***P.O. Box 1500***
***Richland, Washington***



J. D. Randal 01/07/2008
Release Approval Date

**Approved for Public Release;**
**Further Dissemination Unlimited**

Published online November 20, 2007

Vadose Zone Journal · Special Section: Hanford Site

# Impact Assessment of Existing Vadose Zone Contamination at the Hanford Site SX Tank Farm

Raziuddin Khaleel,* Mark D. White, Martinus Oostrom, Marcus I. Wood, Frederick M. Mann, and John G. Kristofzski

The USDOE has initiated an impact assessment of existing vadose zone contamination at the Hanford Site SX tank farm in southeastern Washington State. The assessment followed the Resource Conservation and Recovery Act (RCRA) Corrective Action process to address the impacts of past tank waste releases to the vadose zone at the single-shell tank farm. Numerical models were developed that consider the extent of contamination presently within the vadose zone and predict contaminant movement through the vadose zone to groundwater. The transport of representative mobile (technetium-99) and immobile (cesium-137) constituents was evaluated in modeling. The model considered the accelerated movement of moisture around and beneath single-shell tanks that is attributed to bare, gravel surfaces resulting from the construction of the underground storage tanks. Infiltration, possibly nearing 100 mm $yr^{-1}$, is further amplified in the tank farm because of the umbrella effect created by percolating moisture being diverted by the impermeable, sloping surface of the large, 24-m-diameter, buried tank domes. For both the base case (no-action alternative) simulation and a simulation that considered placement of an interim surface barrier to minimize infiltration, predicted groundwater concentrations for technetium-99 at the SX tank farm boundary were exceedingly high, on the order of $10^6$ pCi $L^{-1}$. The predicted concentrations are, however, somewhat conservative because of our use of two-dimensional modeling for a three-dimensional problem. A series of simulations were performed, using recharge rates of 50, 30, and 10 mm $yr^{-1}$, and compared to the base case (100 mm $yr^{-1}$) results. As expected, lowering meteoric recharge delayed peak arrival times and reduced peak concentrations at the tank farm boundary.

Abbreviations: bgs, below ground surface; BTC, breakthrough curve; RCRA, Resource Conservation and Recovery Act.

The Hanford Site is located on the Columbia River plateau, a semiarid region in south-central Washington State (Fig. 1), with an average annual precipitation of about 180 mm. The site served as a plutonium production facility for nuclear weapons from 1944 to the end of the Cold War era in 1989. A total of 177 large underground tanks were constructed in the Hanford vadose zone to store waste fluid streams from the plutonium extraction facilities. Many of the older single-shell tanks have leaked radioactive waste fluids, posing a contamination hazard for the underlying aquifer and ultimately, the Columbia River. This analysis specifically addresses the SX tank farm (Fig. 1), where highly radioactive and chemically hazardous aqueous fluids of high ionic strength have leaked into the vadose zone. The nature and extent of subsurface contamination; the past, present,

R. Khaleel, Fluor Government Group, P.O. Box 1050, Richland, WA 99352; M.D. White and M. Oostrom, Pacific Northwest National Lab., P.O. Box 999, Richland, WA 99352; M.I. Wood, Fluor Hanford, Inc., P.O. Box 1000, Richland, WA 99352; F.M. Mann and J.G. Kristofzski, CH2M HILL Hanford Group, Inc., P.O. Box 1500, Richland, WA 99352. Received 11 Dec. 2006. *Corresponding author (raziuddin_khaleel@rl.gov).

Vadose Zone J. 6:935–945
doi:10.2136/vzj2006.0176



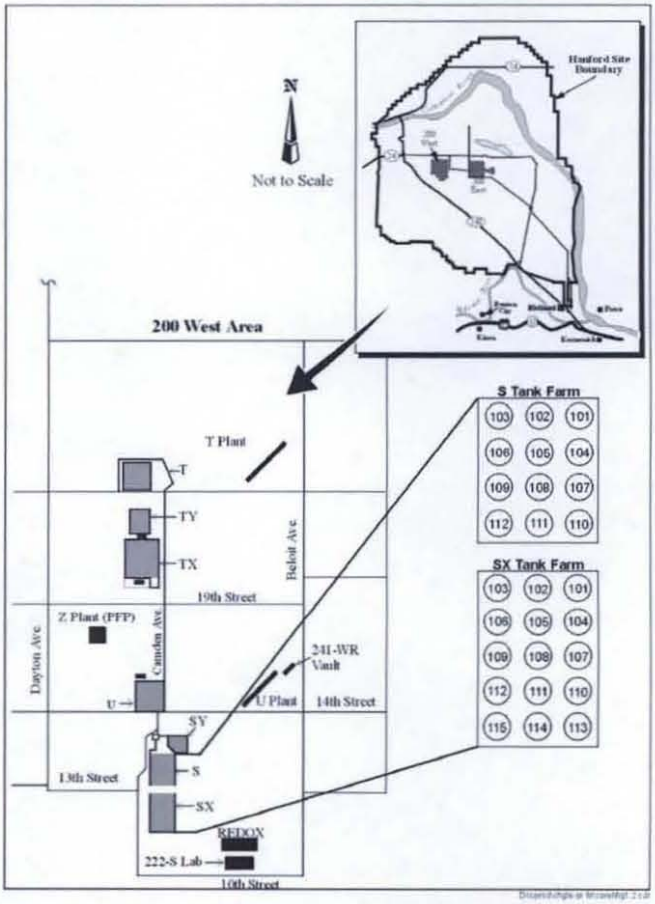


Fig. 1. Location map of single-shell tank Waste Management Area (WMA) S-SX and surrounding facilities in the 200 West Area, Hanford Site, Washington State.

and future migration of contaminants (Pruess et al., 2002); and issues posed by possible future remedial actions are of interest in assessing the impacts associated with the SX tank farm.

The SX tank farm is located within the 200 West Area (Fig. 1). Perturbations of the natural hydrogeologic system at the SX tank farm occurred because the ground was excavated down approximately 15 m below ground surface (bgs), and 15 large cylindrically shaped storage tanks with approximate dimensions of 14-m height and 24-m diameter were emplaced in a regular pattern with about 30-m spacing between tank centers (Fig. 2). The excavated material was then backfilled, and an approximate 2-m gravel layer was placed on top. The altered hydrogeologic properties in the backfilled region led to a substantial increase in net infiltration. The moisture migration within the unsaturated zone was further altered by the umbrella effect of the tanks that diverts moisture around the tank perimeters (Kline and Khaleel, 1995; Ward et al., 1997).

As part of site characterization, a number of studies have been conducted at the S and SX tank farms (Fig. 1). These include characterization of subsurface geology and subsurface conditions (Price and Fecht, 1976; Myers et al., 1998; Johnson et al., 1999; Myers, 2001), vadose zone contamination and contaminant inventories (Raymond and Shdo, 1966; Goodman, 2000; Jones et al., 2000), laboratory investigations (McKinley et al., 2004; Liu et al., 2003; Steefel et al., 2003; Zachara et al., 2002; Serne et al., 2001a, b), and modeling (Ward et al., 1997; White et al., 2001; Pruess et al., 2002; Steefel et al., 2003; Lichtner et al., 2004). A compendium of knowledge on subsurface conditions, hydrogeochemical processes, and nature and extent of vadose zone contamination for the S-SX tank farms has been provided in a recently published field investigation report (Knepp, 2002). Because infiltration is a major driver for transport of long-lived mobile radionuclides (e.g., technetium-99), the report considered several management options for controlling infiltration. One of the management options is emplacement of interim surface barriers to reduce infiltration of moisture and thereby reduce long-term risks from groundwater contamination at the SX tank farm. The objective of our investigation was to evaluate the effectiveness of interim barriers to the infiltration (recharge) of meteoric water (from precipitation and snowmelt) on the migration of contaminants from previous

FIG. 2. 241-SX tank farm under construction.

leak sources. The reference suite of simulations (base case or no-action alternative) considers the migration of contaminants from field estimates of concentration distributions through the vadose zone to the tank farm fenceline boundary with no interim barriers but a closure barrier by the year 2040. The base case results were compared to results for a scenario with an interim barrier placed in 2010, followed by a closure barrier in 2040. The two-dimensional cross-sectional simulations were run for 1000 yr. Two radionuclides, cesium-137 (short-lived with a half-life of 30.14 yr and relatively immobile) and technetium-99 (long-lived with a half-life of $2.03 \times 10^5$ years and mobile) were evaluated. The simulations predicted that cesium-137 does not migrate to the fenceline boundary and that technetium-99 does; therefore, results are presented only for technetium-99.

### Geology and Vadose Zone Contamination Data

The generalized stratigraphy beneath the Hanford Site 200 West Area consists of, in ascending order, the Columbia River Basalt Group, the Ringold Formation, the Cold Creek unit, and the Hanford formation. The geologic cross-section used in two-dimensional cross-sectional modeling for the tank row consisting of tanks SX-107, SX-108, and SX-109 is shown in Fig. 3. Unlike other strata that are comprised of sandy or gravelly sand/sandy

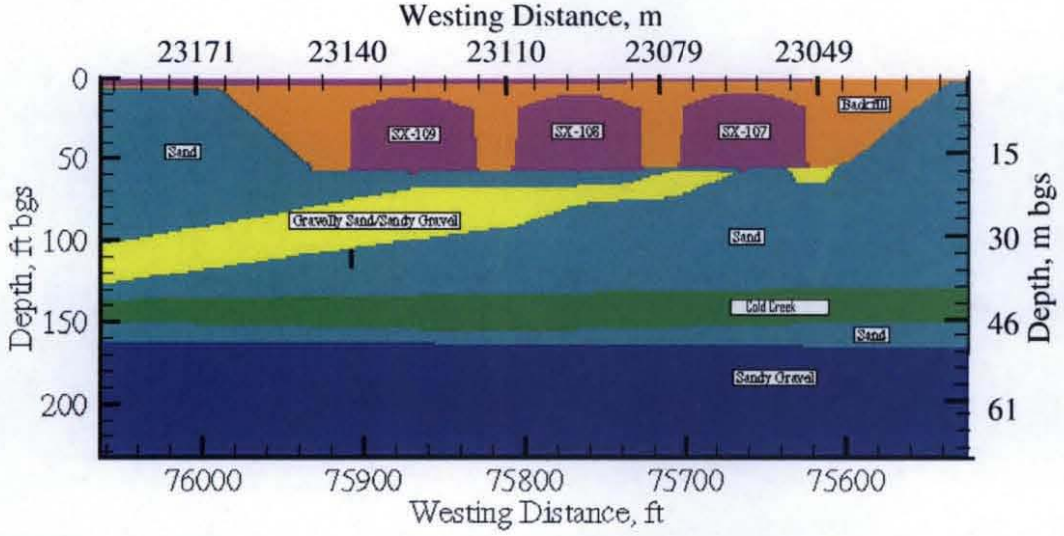


FIG. 3. Geologic cross-section through tank row SX-107, SX-108, and SX-109. Depths and distances are shown in feet (ft) because of its usage at the Hanford Site. (bgs, below ground surface.)

gravel, the Cold Creek unit consists primarily of fine sand and silt and has higher moisture-holding capacity compared with other units. Another noticeable feature of the cross-section is the southwesterly dip of the coarse-grained unit. The fenceline boundary is located on the lower right corner of the cross-section (Fig. 3).

Table 1 provides the estimated contaminant inventory in the vadose zone at the S and SX tank farms. For the tank farm cross-section considered in this study, the vadose zone contamination in the region is dominated by the waste leaked from tank SX-108 between 1962 and 1967. Smaller-volume leaks occurred from tanks SX-107 and SX-109. While other tanks are listed in Table 1, the focus of our study is contamination that is primarily derived from tank SX-108 leak.

TABLE 1. Tank leak volume estimates and estimated contaminant inventory in the vadose zone around the S and SX tank farms.

| Tank | S-104 | SX-107 | SX-108 | SX-109 | SX-113 | SX-115 |
|---|---|---|---|---|---|---|
| Leak volume (L) | 90,840† | 24,035‡ | 57,532‡ | 3,743‡ | 56,775† | 189,250† |
| Constituent (kg) | | | Inventory lost | | | |
| Sodium | 18,200 | 9,900 | 23,700 | 1,540 | 10,500 | 15,700 |
| Aluminum | 3,830 | 2,000 | 4,780 | 311 | 1,950 | 4,240 |
| Chromium | 781 | 471 | 1,130 | 73.3 | 508 | 503 |
| Nitrate ($NO_3$) | 17,000 | 7,400 | 17,700 | 1,150 | 9,960 | 3,870 |
| Nitrite ($NO_2$) | 6,870 | 4,490 | 10,700 | 699 | 3,500 | 9,230 |
| Radionuclides (Ci) | | | Inventory lost | | | |
| Technetium-99 | 3.87 | 5.03 | 12.1 | 0.784 | 2.50 | 5.52 |
| Cesium-137 | 11,400 | 17,100 | 41,000 | 2,670 | 7,340 | 18,800 |

† Leak volumes from Hanlon (2001).
‡ Leak volumes based on Jones et al. (2000).

In 1998 borehole 41-09-39 (W23-234 in Fig. 4), located near tank SX-108, was sampled in two episodes following its initial completion. First, the borehole was extended via drilling from about 39.6 m (130 ft) bgs to groundwater, about 65.5 m (215 ft) bgs, with near continuous sampling obtained during the extension. Then the upper portion was sampled via coring of borehole sidewall from 39.6 to 7.6 m (130–25 ft) bgs as the borehole was decommissioned; the sidewall core samples were of 2.5 × 2.5 × 28 cm.

A slant (~30° off vertical) borehole (W23-64 in Fig. 4) was also drilled near tank SX-108. Sixteen core samples were recovered from the slant borehole at depths from 16.8 to 43.9 m (55–144 ft) bgs. The sediment characterization data were augmented with spectral gamma logging data from 98 drywells (not shown) surrounding the SX tanks. The spectral gamma logs show that the vast majority of the cesium-137 is in the upper regions of the vadose zone between 0 and 12.2 m (40 ft) below the tank bottoms, that is, 16 to 28.3 m (53–93 ft) bgs, and within the coarse-grained unit that dips to the southwest (Fig. 3). Some cesium-137, however, is present as deep as 30.5 m (100 ft) below the tank bottoms in several places.

The sediment characterization data from the recent boreholes show that the bulk of the cesium-137 under tank SX-108 is found between 0 and 12.2 m (40 ft) below the tank bottom, that is, 16 to 28.3 m (53–93 ft) bgs. At borehole 41-09-39, the bulk of the cesium-137 is found between 1.8 and 16.8 m (6–55 ft) below tank bottoms, that is, 18 to 33 m (59–108 ft) bgs. Figure 5 shows the vadose

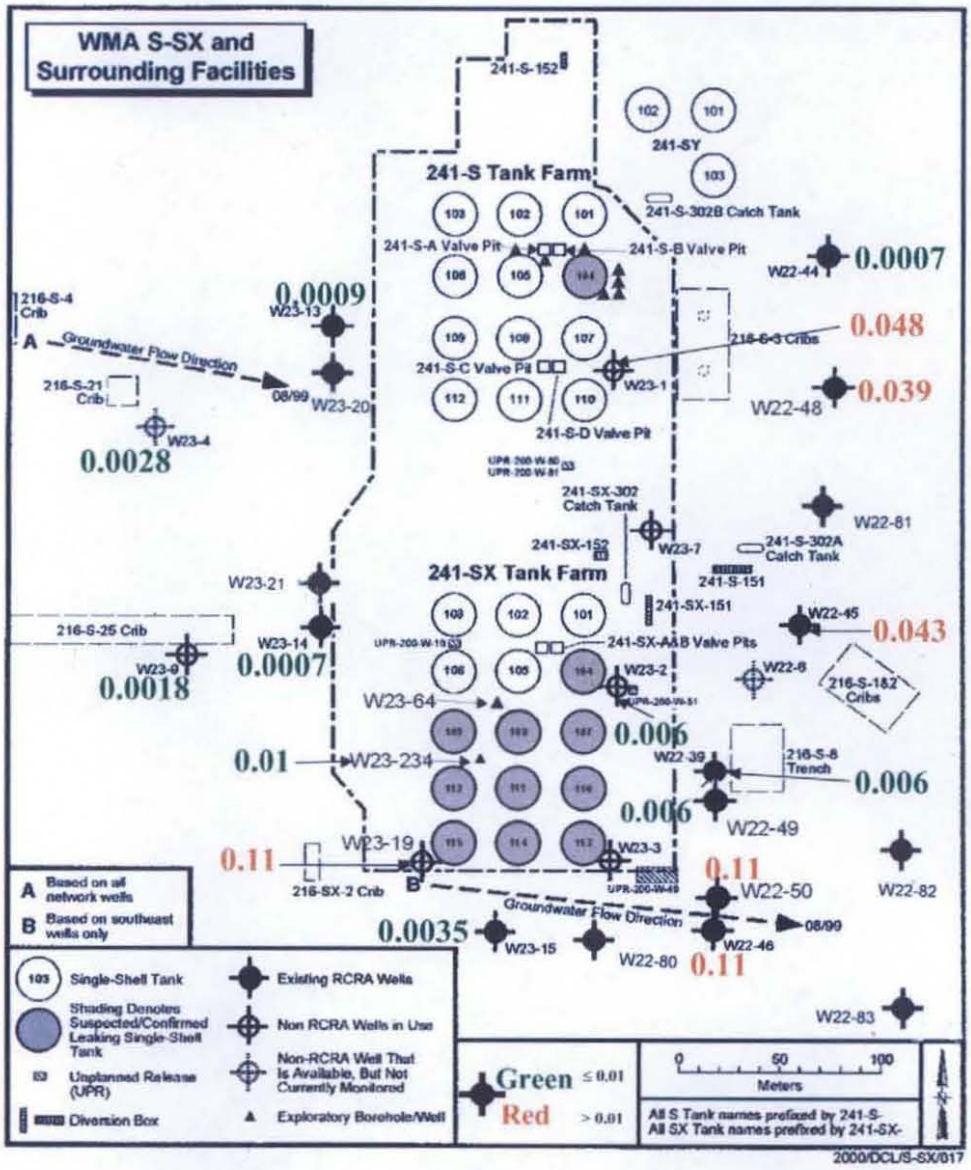


FIG. 4. Technetium-99/(nitrate + nitrite) ratios for Waste Management Area (WMA) S-SX network wells (the ratios highlighted in green and red). The technetium-99/(nitrate + nitrite) ratios for tanks SX-108 and SX-115 are 0.43 and 0.42 pCi $\mu g^{-1}$, respectively. All well numbers are prefixed by 299-. RCRA = Resource Conservation and Recovery Act.

zone contaminant profiles for cesium-137, technetium-99, and sodium, based on borehole 41-09-39 sampling for tank SX-108 leak. As described below, Fig. 5 is primarily used to develop initial conditions for vadose zone contaminant distribution.

### Conceptual Model for Migration of Tank Leak

Historically, it was assumed that cesium-137 sorbs readily on to Hanford sediments, drops out of solution quickly, and hence is not available for transport through the vadose zone. However, in the SX tank farm, cesium-137 was found farther into the vadose zone than the preceding hypothesis would suggest. An extensive effort (Serne et al., 2001a, b) to understand this observation was undertaken, and it was found that for tank leak SX-108, supernate chemistry controlled the local chemical environment near the leak. Historical knowledge of tank supernate chemistry and laboratory sorption work (McKinley et al., 2004; Liu et al., 2003; Zachara et al., 2002), as well as numerical calculations (Steefel et al., 2003; Lichtner et al., 2004), indicated that optimum conditions existed at the time of tank leak to cause higher-than-postulated cesium-137 mobility. The primary enabling conditions were a combination of very high sodium and cesium-137 concentrations in tank fluid. Under these conditions, sodium was more strongly sorbed, causing cesium-137 to remain in solution.

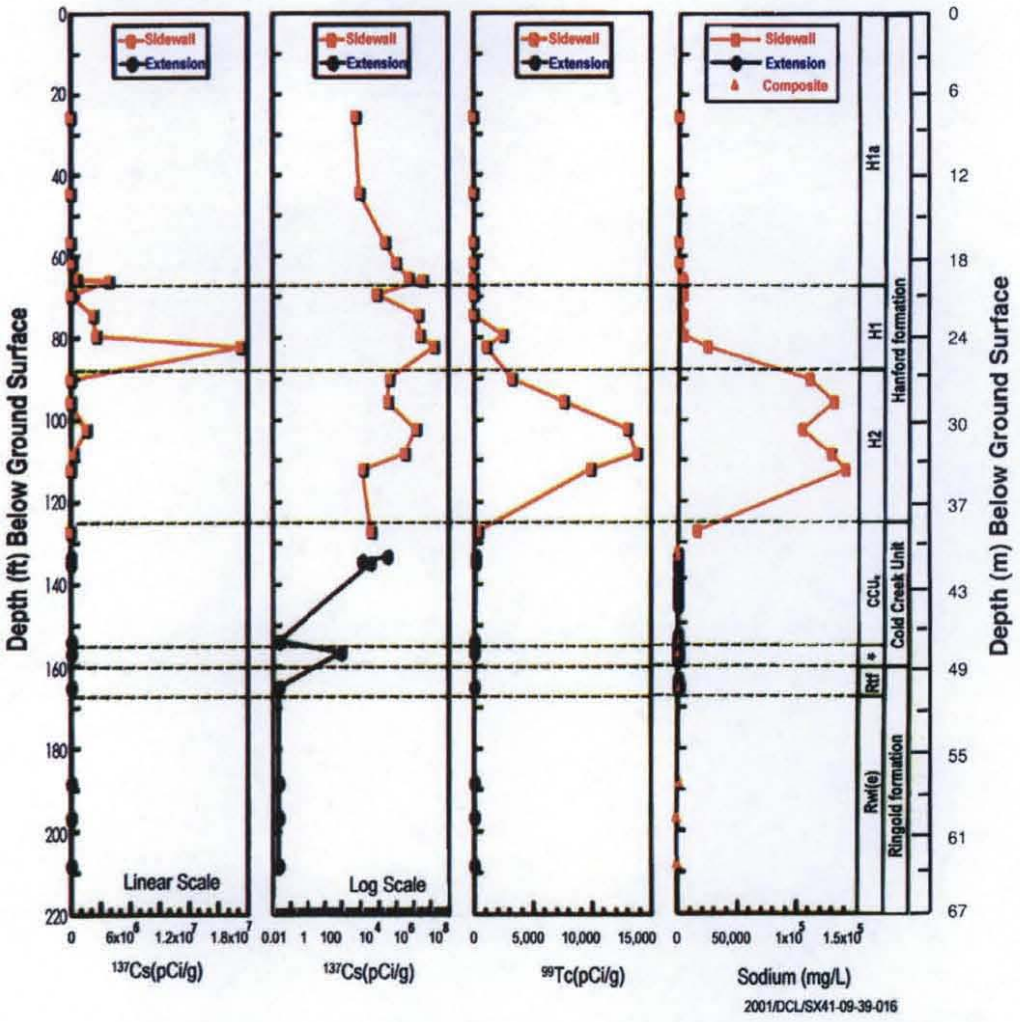


FIG. 5. Vadose zone contamination for cesium-137, technetium-99, and sodium near tank SX-108 (after Serne et al., 2001a). A composite sample is obtained by combining two adjacent sleeves of the borehole liner. Depths are shown in feet (ft) because of its usage at the Hanford Site.

From these observations, a simplified two-step model for how the SX-108 leak migrated into the vadose zone was postulated. In the first step, a rather rapid release of the leaking fluid occurred, providing a hydraulic driver for the fluid to move through the vadose zone. Stratigraphic variability in the vadose zone geology exerted sufficient influence to induce movement initially in the lateral direction to the southwest (Fig. 3). The supernate chemistry controlled the local geochemical conditions to enhance the mobility of cesium-137 so that the cesium was poorly retarded and migrated essentially with the leaking tank fluid. As discussed in Serne et al. (2001a), the ratio of cesium-137 to technetium-99 activity in the shallow sediments from 18.3 to 25 m (60–82 ft) bgs was greater than 10,000. Such high ratios suggest that cesium-137 and technetium-99 may be traveling at the same rate through these shallow sediments below the tank bottom. However, the potential exists that the presence of some of the cesium-137 in deep vadose zone sediments is due to drag-down (push-down) along the borehole.

In the second step, the hydraulic driver for the leak event eventually relaxed, and the moisture distribution within the far-field (away from the leak source and at depths in excess of 10 m below tank bottom) vadose zone equilibrated with natural infiltration. Far-field conditions reverted to more natural soil-water conditions (the soil essentially buffered the high sodium tank chemistry), thus again causing cesium-137 to sorb strongly to sediments. As indicated in Fig. 5, subsequent movement of cesium-137 was held to a minimum. Between the depths of 27.4 and 40.9 m (90 and 134 ft) bgs, the cesium-137 to technetium-99 ratio ranges from less than 1 to about 100 (Serne et al., 2001a), which suggests that cesium-137 eventually is removed from the fluid. However, technetium-99 as well as other non-sorbing constituents (e.g., nitrate, nitrite, and sodium) remained mobile. Figure 5 shows a reduction of sodium concentration and a distinct chromatographic separation of cesium-137 and sodium with depth. Once cesium-137 and sodium were sufficiently separated, cesium-137 sorption became favorable, fixing it in place. Site characterization data (Fig. 5) also suggest that the bulk of the radionuclide inventory from the SX-108 leak is still within the vadose zone and, as discussed below, only a small fraction of contamination from the leak reached the unconfined aquifer.

## Modeling Approach

The simulations in this study did not model the impact of a tank leak itself but modeled the impact from past tank leaks, as quantified by existing contamination within the vadose zone (Fig. 5). All simulations were composed of steady-flow and transient components, where flow fields developed from the steady-flow component were used to initialize the transient simulation. From the starting conditions, transient simulations of solute transport were conducted for a 1000-yr period (i.e., year 2000 CE to 3000 CE) that involved changes in the flow fields in response to placement of surface barriers.

Fluid flow within the vadose zone was described by Richards' equation, whereas the contaminant transport was described by the conventional advective–dispersive transport equation with an equilibrium linear sorption coefficient ($K_d$) formulation. Data on laboratory measurements for moisture retention, particle-size distribution, saturated and unsaturated hydraulic conductivity, and bulk density for individual stratum were based on samples from 200 East and 200 West Areas (Khaleel et al., 2000; Khaleel and Freeman, 1995). Samples that contained measurements of soil moisture retention as well as unsaturated hydraulic conductivity were used. This was primarily to avoid extrapolating unsaturated conductivities (van Genuchten, 1980; Mualem, 1976) to the dry end, based on moisture retention and saturated conductivity estimate (Khaleel et al., 1995). Also, to reflect field conditions, the laboratory data were corrected for the presence of any gravel fraction in the sediment samples (Khaleel and Relyea, 1997). As with flow modeling, each stratum was modeled with a range of transport parameters (i.e., bulk density, diffusivity, and macrodispersivity).

### Initial Conditions for Flow

Steady-state initial conditions were developed by simulating from a prescribed unit hydraulic gradient condition to a steady-state condition, dictated by the initial meteoric recharge at the surface, variation in soil hydraulic properties, location of impermeable tanks, and no flux vertical boundaries above the water table. The water table boundary was prescribed by the water table elevation (65.5 m [215 ft] bgs) and an unconfined aquifer hydraulic gradient (0.0012 m $m^{-1}$) from west to east. No-flux boundaries were used for the lower boundary (Fig. 3). No solute transport was considered during the steady-state simulation.

### Model Setup and Boundary Conditions

A two-dimensional (west–east) vertical (x–z) slice of the flow domain was used for modeling flow and transport. The flow domain includes the tank farm fenceline boundaries and extends vertically from the ground surface to about 6 m below the water table. The geologic strata are assumed continuous but not of constant thickness. For flow modeling, Neumann boundary conditions are prescribed at the surface with the flux equal to the recharge rate estimate. For transport modeling, a zero flux boundary was prescribed at the surface for cesium-137 and technetium-99. Above the water table, the western and eastern boundaries were assigned no-flux boundaries for both flow and transport.

### Recharge Estimates, Flow and Transport Parameters, and Inventory Estimates

This section provides the recharge estimates as well as the effective (upscaled) values of flow and transport parameters for the vadose zone. Specific flow parameters include moisture retention and saturated and unsaturated hydraulic conductivity. Transport parameters include bulk density, diffusivity, sorption coefficient for cesium-137, and macrodispersivity. Details on deriving the effective (upscaled) parameters are addressed in Khaleel et al. (2000). The section concludes with how the contaminant inventory was assigned as a function of elevation within the vadose zone.

#### Recharge Estimates

The tank farm surfaces are covered with gravel to prevent vegetation growth and provide radiation shielding for site workers. Bare gravel surfaces, however, enhance net infiltration of meteoric water compared with undisturbed naturally vegetated surfaces (Gee et al., 1992). Infiltration is further enhanced in the tank farms by the effect of percolating water being diverted by the impermeable, sloping surface of the tank domes. The basis for recharge estimates (Table 2) is presented in Khaleel et al. (2000).

#### Effective Flow Parameters

Table 3 lists the composite, fitted van Genuchten–Mualem parameters (van Genuchten, 1980) for various strata at the tank farm. As stated above, to obtain a better fit for unsaturated conductivity for the moisture regime of interest, the parameters are based on a simultaneous fit of both moisture retention and unsaturated conductivity data so that the saturated hydraulic conductivity, $K_s$ (Table 3) is a fitted parameter, not the laboratory-measured value. Also, because of a lack of information, sandy gravel data were used to represent properties for backfill sediments.

The modeling accounts for moisture- or tension-dependent anisotropy (Yeh et al., 1985) for Hanford sediments. The hetero-

TABLE 2. Estimated recharge for interim and closure barriers.

| Condition simulated | Recharge estimate |
|---|---|
| | mm $yr^{-1}$ |
| No barrier (2000–2010) | 100 |
| Interim barrier (2010–2040) | 0.5 |
| Closure barrier (first 500 yr) (2040–2540) | 0.1 |
| Degraded closure barrier (post 500 yr) (2540–3000) | 3.5 |

TABLE 3. Average bulk density and composite van Genuchten–Mualem parameters for various strata.†

| Strata | Number of samples | Bulk density | $\theta_s$ | $\theta_r$ | $\alpha$ | $n$ | $l$ | $K_s$ |
|---|---|---|---|---|---|---|---|---|
| | | g $cm^{-3}$ | | | $cm^{-1}$ | | | cm $s^{-1}$ |
| Backfill | 10 | 1.94 | 0.1380 | 0.0100 | 0.0210 | 1.3740 | 0.5 | 5.60E-04 |
| Sand | 12 | 1.76 | 0.3819 | 0.0443 | 0.0117 | 1.6162 | 0.5 | 0.99E-04 |
| Gravelly sand/sandy gravel | 11 | 2.07 | 0.2126 | 0.0032 | 0.0141 | 1.3730 | 0.5 | 2.62E-04 |
| Cold Creek | 4 | 1.65 | 0.4349 | 0.0665 | 0.0085 | 1.8512 | 0.5 | 2.40E-04 |
| Sandy gravel | 10 | 2.13 | 0.1380 | 0.0100 | 0.0210 | 1.3740 | 0.5 | 5.60E-04 |

† $\theta_s$ = saturated moisture content, $\theta_r$ = residual moisture content, $\alpha$, $n$ = van Genuchten parameters, $l$ = pore connectivity parameter, $K_s$ = saturated hydraulic conductivity. Note that $K_s$ is not the laboratory measured value but is a fitted parameter to obtain an accurate fit for unsaturated conductivity for the drier moisture regime of interest.

geneous nature of Hanford sediments is effective in smearing out the effects of large natural or manmade water applications. This was illustrated by the moisture content profiles at a controlled field injection experiment site in the 200 East Area (Sisson and Lu, 1984; Ward et al., 2000; Ye et al., 2005). The field data for the injection experiment also suggests moisture- or tension-dependent anisotropy (Yeh et al., 2005; Ward et al., 2006). Variable, tension-dependent anisotropy provides a framework for upscaling laboratory-scale measurements to the effective (upscaled) properties for the large-scale tank farm vadose zone.

The Polmann (1990) model was used to describe tension-dependent anisotropy for sediments at the tank farm; details are in Khaleel et al. (2000, Appendix C). To account for moisture-dependent anisotropy, the Gardner (1958) relationship was used to describe unsaturated hydraulic conductivity ($K$) as a function of $K_s$ and tension, $h$. The Gardner model is referred to as the log-linear model, because $\ln K$ is linearly related to $h$ through the Gardner slope $\beta$, the pore-size distribution parameter. However, such a constant slope is often inadequate in describing $\ln K(h)$ over ranges of tension of practical interest for field applications. Therefore, the slope $\beta$ was approximated locally by straight lines over a fixed range of tension. The $\ln K_s$ in Gardner equation was then derived by extrapolating the local slopes back to zero tension.

Using a linear correlation relationship between the log-conductivity zero-tension intercept and $\beta$, the Polmann (1990) generalized model accounts for the cross-correlation of the local soil property (i.e., $\ln K_s$ and $\beta$) residual fluctuations. Compared to the uncorrelated $\ln K_s$ and $\beta$ model (Yeh et al., 1985), a partial correlation of the properties has a significant impact on the magnitude of the effective parameters derived from the stochastic theory.

### Effective Transport Parameters

Similar to flow parameters, because of natural variability, the transport parameters are spatially variable. The purpose was again, similar to the flow parameters, to include the effect of such variability on the large-scale transport process.

The average bulk density estimates (Table 3) were based on data in Khaleel et al. (2000) for the five strata. A sorption value of 500 mL $g^{-1}$ was used for cesium-137 (Kaplan and Serne, 1999) as being representative of undisturbed sediments. The sorption coefficient for technetium-99 was estimated to be zero. The effective, large-scale diffusion coefficients for tank farm soils were assumed to be a function of volumetric moisture content, $\theta$, and are expressed using an empirical relation (Millington and Quirk, 1961).

Macrodispersivities were defined in a manner similar to saturated media estimates (Gelhar and Axness, 1983). Macrodispersivity estimates are needed for both reactive (i.e., cesium-137) and nonreactive (i.e., technetium-99) species. The estimates are different for cesium-137 than those for technetium-99 because, unlike nonsorbing technetium-99, the sorption for cesium-137 varies as the soil properties experience spatial variability (Gelhar, 1993; Talbott and Gelhar, 1994). Such variation affects the contaminant velocity, which, in turn, enhances the spreading of the plume. For reactive species (cesium-137), the enhanced spreading is defined by a macrodispersivity enhancement, relative to spreading for nonreactive (technetium-99) species.

An extended review is provided in Khaleel et al. (2000) on the rationale for macrodispersivity estimates; Table 4 gives the nonreactive estimates for technetium-99. The transverse values were estimated to be 10% of the longitudinal macrodispersivities. For cesium-137, the macrodispersivity enhancement ranged from about 1.07 for backfill sediments to about 2.35 for Cold Creek unit sediments. Stochastic theory (Gelhar, 1993) indicates that the macrodispersivity enhancement only occurs in the longitudinal direction.

TABLE 4. Nonreactive longitudinal ($A_L$) and transverse ($A_T$) macrodispersivity estimates for various strata for technetium-99.

| Strata | $A_L$ | $A_T$ |
|---|---|---|
| | cm | |
| Backfill | 150 | 15 |
| Sand | 150 | 15 |
| Gravelly sand | 100 | 10 |
| Cold Creek | 50 | 5 |
| Sandy gravel | 150 | 15 |

### Inventory Assignment by Depth

Figure 5 was used to assign inventory within the vadose zone profile. First, the estimated inventory (Table 1) in the vadose zone due to contribution from tanks SX-108 and SX-109 were added; the total inventory under both tanks was then distributed in the lateral direction across the two tanks (including the space between the tanks) (Fig. 6a and 7a). For tank SX-107, the inventory is distributed across the diameter of that tank only (Fig. 7a).

Next, both contaminant concentration (Fig. 5) and mass (Table 1) were constrained in distributing the inventory in the lateral direction for each depth within the vadose zone. In assigning the contaminant inventory by depth, it was assumed that higher inventories are associated with higher concentrations. Thus, the depth distribution consisted of a series of concentric disks of varying concentration and diameter with depth (Fig. 7a); the disk diameter was sized to maintain the total solute mass for a particular depth. Note that Fig. 5 is based on borehole 41-09-39 data; contaminant concentrations were slightly higher at borehole 41-09-39, compared to those at the slant borehole.

## Numerical Simulation Results

All simulations reported herein were performed using the STOMP simulator (White and Oostrom, 2000a, 2000b). A detailed discussion on the numerical implementation for STOMP and simulation results is presented in White et al. (2001). Selected results are summarized in Fig. 6 through 12 and are discussed below.

### Base Case: No Action Alternative

The base case simulation investigated solute transport considering natural surface infiltration, no interim surface barriers, but with a closure barrier by the year 2040. The closure barrier limits infiltration to 0.1 mm $yr^{-1}$ for the first 500 yr. The simulations were initialized using a steady-state flow solution defined by a surface recharge rate of 100 mm $yr^{-1}$ and a hydraulic gradient in the unconfined aquifer. Simulated results are presented for relative saturation ($\theta/\theta_s$ where $\theta$ = moisture content and $\theta_s$ = saturated moisture content) distribution as well as for the solute concentration distribution for years 2000, 2050, 2540, and

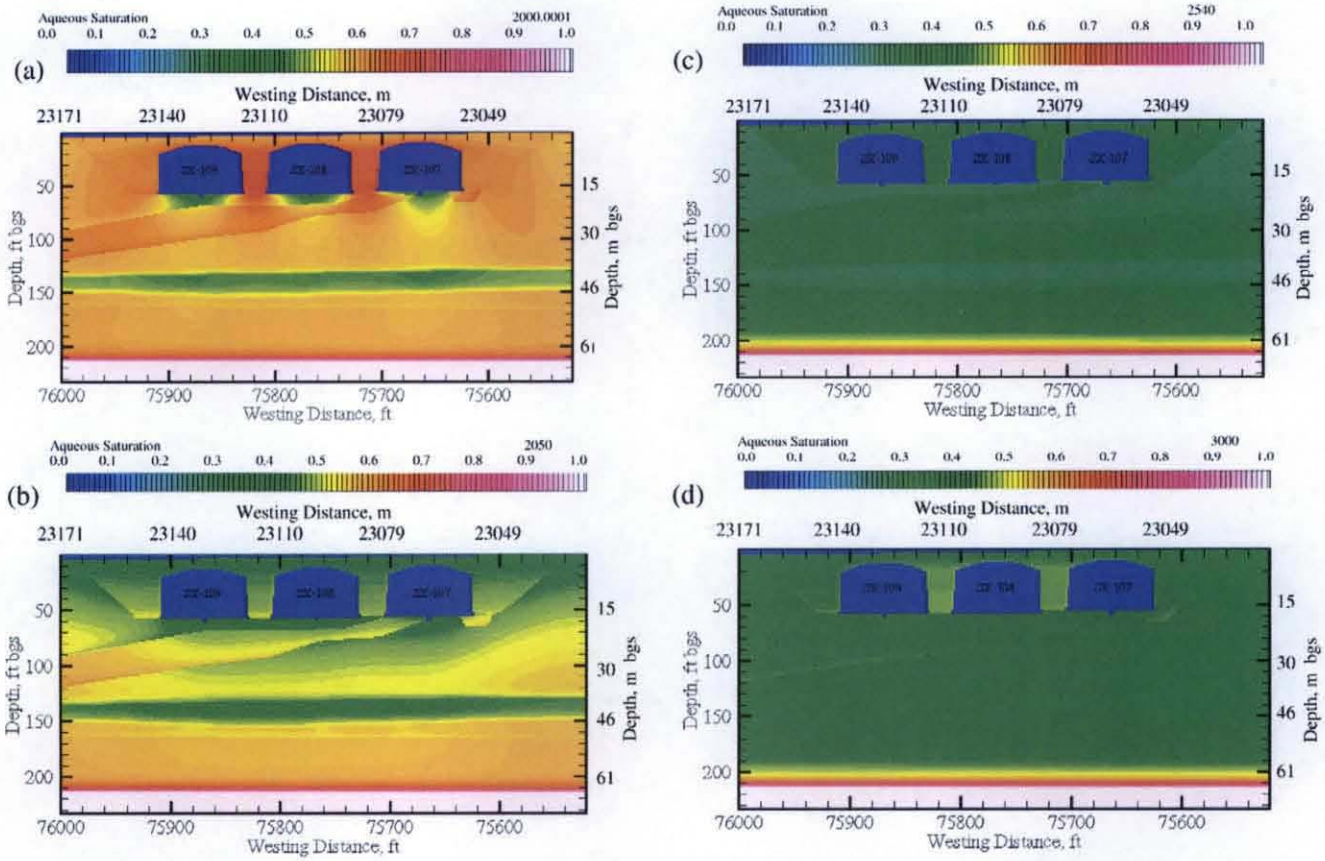


FIG. 6. Progression of saturation profile at year (a) 2000, (b) 2050, (c) 2540, and (d) 3000. Depths and distances are shown in feet (ft) because of its usage at the Hanford Site. (bgs, below ground surface.)

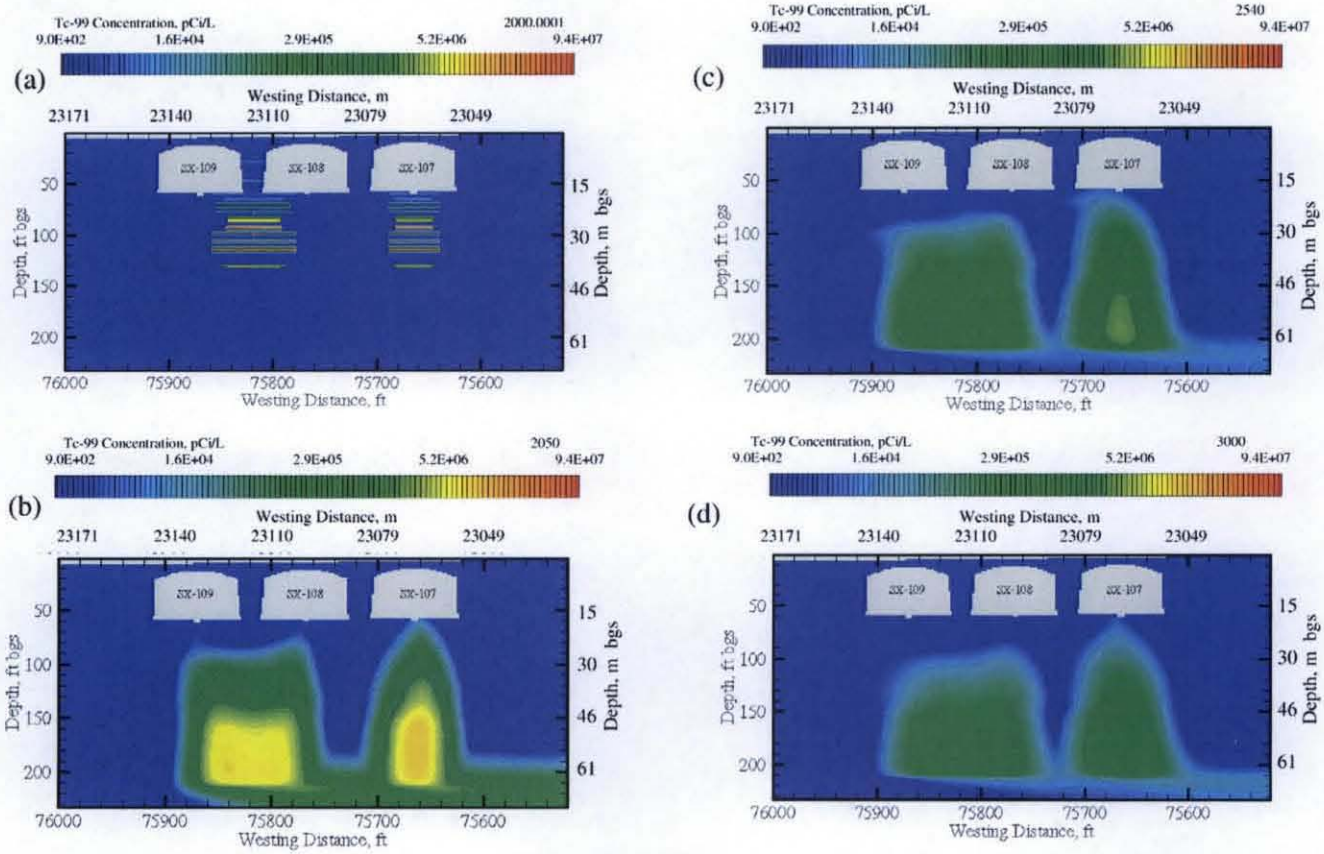


FIG. 7. Progression of technetium-99 distribution at year (a) 2000, (b) 2050, (c) 2540, and (d) 3000. Depths and distances are shown in feet (ft) because of its usage at the Hanford Site. (bgs, below ground surface.)

3000. The moisture content field for these simulations remains unchanged from the initial steady-flow field until the year 2040, when the closure barrier becomes effective.

The saturation field is dependent on the surface recharge, impermeable structures (e.g., single-shell tanks), various strata, and their hydraulic parameters. The steady-flow saturation field with 100 mm $yr^{-1}$ of meteoric recharge is shown in Fig. 6a. This field shows the impact of the tanks on the relative saturation, where higher than ambient saturations occur above and between the tanks and lower than ambient saturations occur just below the tanks.

By 2040 a closure barrier was assumed to be active, which lowered the meteoric recharge from 100 mm $yr^{-1}$ to 0.1 mm $yr^{-1}$. The saturation field dried in response to the change in surface recharge, as shown in Fig. 6b for the year 2050. A comparison of Fig. 6a and 6b shows that, at a lower value of surface recharge, the impact of the impermeable tanks on saturation is reduced. The closure barrier was assumed to remain effective for 500 yr, at which point it degrades, allowing meteoric recharge to increase to 3.5 mm $yr^{-1}$. In the 500-yr period between 2040 and 2540, the saturation field continued to slowly dry reaching a minimum average level at 2540, as shown in Fig. 6c. In the 460-yr period between 2540 and 3000, the saturation field wetted, in response to the increased meteoric recharge of 3.5 mm $yr^{-1}$ for the degraded surface barrier. The saturation field at year 3000 is shown in Fig. 6d. The closure barrier was assumed to decrease the meteoric recharge from 100 mm $yr^{-1}$ to 0.1 mm $yr^{-1}$ for 500 yr and then degrade to 3.5 mm $yr^{-1}$ for the next 460 yr. The variations in surface infiltration had the greatest impact on saturation in the region between tanks within the backfill material and the region immediately below the bottom of the tanks. As evident from Fig. 6a to 6d, the Cold Creek unit showed the least change in saturation with change in the surface recharge. The regions directly beneath the tanks additionally showed lower variability in relative saturation.

Color-scaled images for technetium-99 are shown as a series of time sequences in Fig. 7a to 7d. The solute concentrations are color valued using exponential scaling from the maximum concentration limit of 900 pCi $L^{-1}$ for technetium-99 to the maximum initial inventory concentration. Note the differences in time sequences (Fig. 7a–7d); the initial inventory was spread across the region between tanks SX-108 and SX-109 and centered beneath tank SX-107. Although differences are noticeable in the plume located between tanks SX-109 and SX-108 with the plume beneath tank SX-107, the overall rate of migration toward the groundwater is nearly identical. The initial inventory beneath tank SX-107 shows a slight delay in arrival times. Some variations in solute migration direction are noted due to the sloped gravelly sand strata, but none substantially alter the breakthrough concentrations at the SX fenceline boundary, located on the lower right-hand corner of the domain (Fig. 7a–7d).

Figure 8 illustrates the simulated water flux at the water table as a function of time, whereas Fig. 9 shows the solute breakthrough curve (BTC) for technetium-99 at the tank farm fenceline. No cesium-137 was transported to the fenceline boundary for the simulated cross-section. This is true for the base case as well as for the interim barrier case.

### Interim Barrier Case

The interim barrier case investigated solute transport considering natural surface infiltration, an interim surface barrier placed in the year 2010, and a closure barrier in the year 2040. Unlike the closure barrier, which limits the infiltration rate to 0.1 mm $yr^{-1}$ for the first 500 yr, the interim barrier limits the infiltration rate to 0.5 mm $yr^{-1}$. Again, the simulations were initialized using a steady-state flow solution defined by the surface recharge rate of 100 mm $yr^{-1}$ and a hydraulic gradient in the unconfined aquifer. Inventories for the two contaminant species and their distribution within the vadose zone were identical to those for the base case. The moisture content field for these simulations remains unchanged from the initial steady-flow. Figure 10 illustrates the simulated water flux at the water table as a function of time, whereas Fig. 11 shows the solute BTC for technetium-99 at the tank farm fenceline.

Breakthrough times and peak technetium-99 concentrations at the tank farm fenceline boundary are shown in Table 5 for cases with and without interim barrier. For comparison, maximum initial concentrations are also included in Table 5. Results indicate that, compared with the base case, the interim surface barrier reduces solute concentration at the tank farm fenceline but has negligible impact on the technetium-99 peak concentration arrival time. Although results are not shown here, the

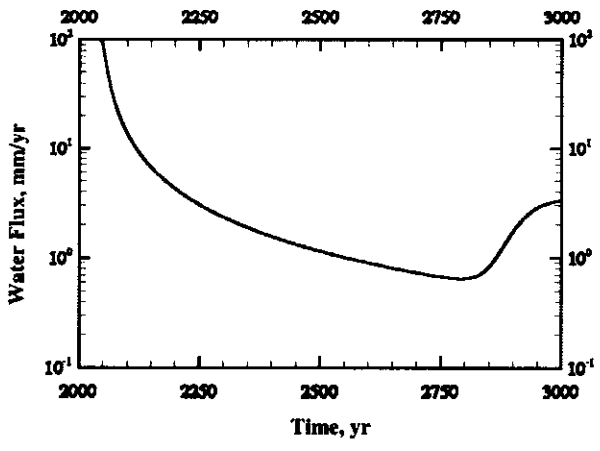


FIG. 8. Simulated flux versus time at the water table for the base case with no interim barrier.

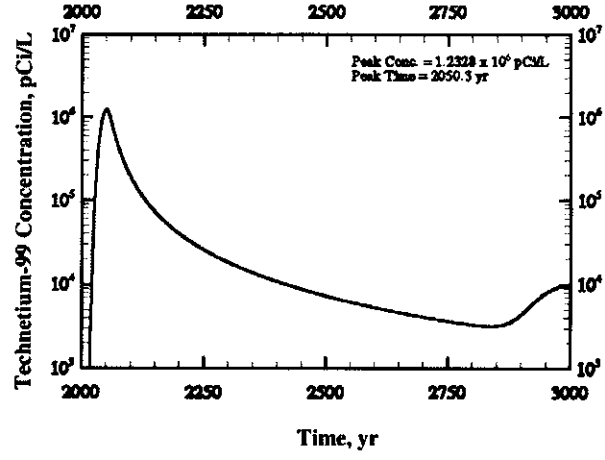


FIG. 9. Simulated breakthrough curve for technetium-99 at the tank farm fenceline for the base case with no interim barrier.

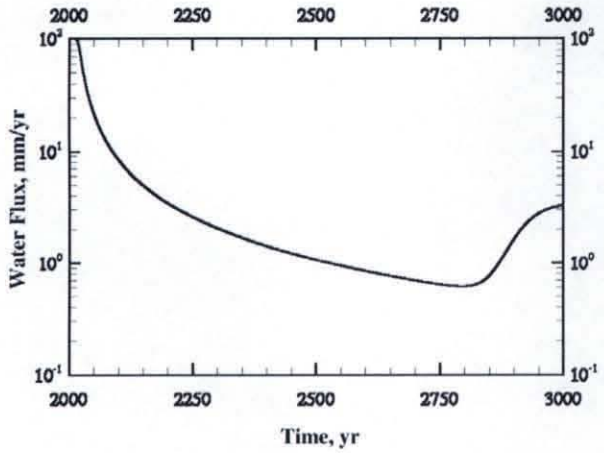


FIG. 10. Simulated flux versus time at the water table for the interim barrier case.

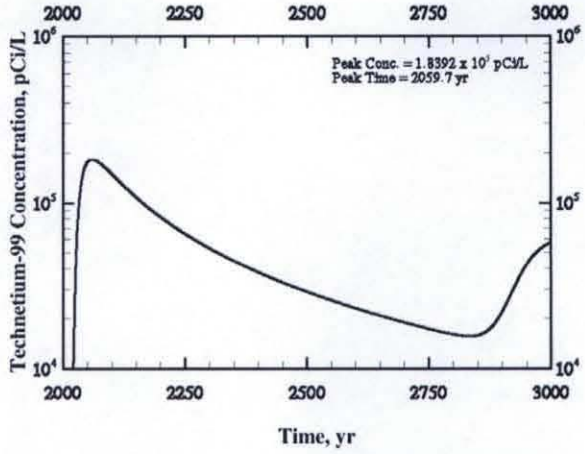


FIG. 11. Simulated breakthrough curve for technetium-99 at the tank farm fenceline for the interim barrier case.

impact of the interim surface barrier on lowering peak concentrations is most affected by the initial vadose zone contaminant inventory distribution. Inventory distributions having concentrations of solute mass nearer the water table were less affected by the interim barrier compared with the inventory mass located higher up in the vadose zone. Concentrations at the fenceline boundary at year 3000 were always higher for the interim barrier simulation compared with the base case simulation, which indicates that a major benefit of the interim barrier is to dampen the technetium-99 flux into the aquifer, broaden the breakthrough curve at the fenceline, and reduce peak concentrations.

### Impact of Recharge Rates

To investigate the impact of meteoric recharge on contaminant transport, a series of simulations were performed, using recharge rates of 50, 30, and 10 mm $yr^{-1}$, and compared to the base case (100 mm $yr^{-1}$) results. In all cases, the closure barrier was assumed to control recharge beyond the first 40 yr. The initial flow field for these simulations was the steady-state condition for the prescribed meteoric recharge rate and fixed groundwater conditions (i.e., water table conditions and gradient). As expected, lowering meteoric recharge delayed peak arrival times and reduced peak concentrations at the fenceline boundary (Fig. 12). The exception was the 10 mm $yr^{-1}$ recharge case (Fig. 12), where arrival times were delayed beyond 1000 yr. However, because of the late arrival, the peak concentrations for the low-recharge case continued to increase for the 1000-yr simulation. Nonetheless, the concentration at the boundary, after 1000-yr simulation, was still well below those for other recharge rates.

All preceding simulations were performed using an isothermal model. Such an assumption is supported by a comparison of simulation results for nonisothermal and isothermal runs (White et al., 2002). Nonisothermal model simulations indicate that during periods of high heat loads in the 1950s and 1960s, the thermal load from the boiling waste tanks altered flow patterns and caused large-scale redistribution of moisture. As a result, fluid and vapor flow near the high-heat tanks was dominated by vapor–liquid counterflow. To understand the historical behavior, it is therefore important to consider the strong coupling between the thermal and hydrologic environments. For impact assessment, however, long-term simulation results for technetium-99 migration for isothermal and nonisothermal conditions were not significantly different (White et al., 2002), despite the known thermal effects of high-heat tanks.

TABLE 5. Simulated peak concentrations and arrival times for technetium-99 at the tank farm fenceline.

| Parameter | Base case with no interim barrier | Interim barrier case |
|---|---|---|
| Arrival time (yr) | 2050.3 | 2059.7 |
| Peak concentration (pCi $L^{-1}$) | $1.233 \times 10^6$ | $0.1839 \times 10^6$ |
| Max. initial concentration (pCi $L^{-1}$)† | $94.80 \times 10^6$ | $94.80 \times 10^6$ |

† Soil concentrations (pCi $g^{-1}$ soil) were converted to aqueous-phase concentrations based on the soil bulk density and the initial moisture content.

### Comparison of Base Case Model Results with Other Studies

Ward et al. (1997) investigated technetium-99 transport due to tank leaks for the same cross-section considered in this study. Their modeling approach, however, was different from ours. Unlike ours, they modeled tank leaks, whereas we used the existing vadose zone contamination as our initial condition for technetium-99 migration through the vadose zone and on to groundwater. Ward et al. (1997) found that, in addition to leak volume estimates and fluid density estimates of the leaked waste, recharge rates had a significant impact on technetium-99 migration. Under high recharge rates, technetium-99 migrated

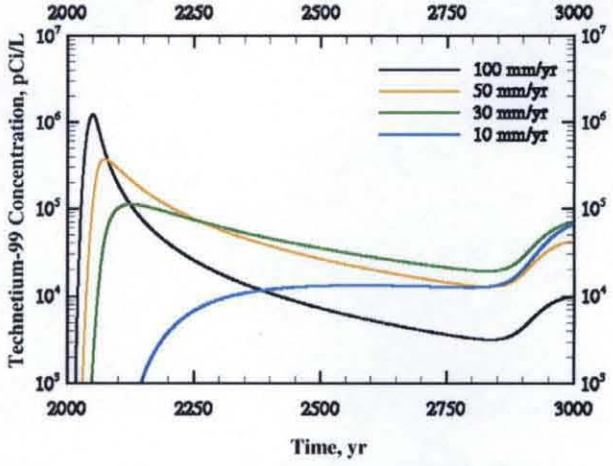


FIG. 12. Simulated breakthrough curves for technetium-99 at the tank farm fenceline for various recharge estimates.

rapidly to the water table, arriving within 30 yr of the initial leak. For a leak volume of 500 kL (132,000 gal), depending on recharge rates and specific gravity of leaked fluid (1.0 to 1.4), their simulated technetium-99 peak porewater concentrations at the water table were in the range of $2 \times 10^6$ to $12 \times 10^6$ pCi $L^{-1}$. Because of groundwater mixing, our simulated peak concentration at the tank farm fenceline is lower (Table 5) but within the same order of magnitude of Ward et al. (1997) results for the no-action alternative.

With respect to field data, RCRA monitoring wells (Fig. 4) in the vicinity of waste management area (WMA) S-SX show evidence of groundwater contamination from tank waste sources. Downgradient of the tanks to the south and east, technetium-99/(nitrate + nitrite) ratios are elevated with respect to those samples analyzed in upgradient wells to the west and north. With relatively greater technetium-99 inventories present in tank leak fluids compared with neighboring cribs and trenches, the difference in ratios is attributed to contribution from tank waste sources. However, current contributions are limited and have depleted little of the vadose zone source term. For example, the field evidence indicates that the bulk of technetium-99 is relatively high up in the vadose zone (e.g., technetium-99 distribution in borehole 41-09-39 [Fig. 5]).

We hypothesize that current contamination in the unconfined aquifer is a small fraction of the initial inventory and has reached the aquifer because of even more severe, but short-term and more localized, recharge events than those assumed in the modeling. The technetium-99/(nitrate + nitrite) ratios for tanks SX-108 and SX-115 are 0.43 and 0.42 pCi $\mu g^{-1}$, respectively. Maximum technetium-99 concentrations and technetium-99/(nitrate + nitrite) ratios (e.g., 188,000 pCi $L^{-1}$ and 0.11 pCi $\mu g^{-1}$) in well 299-W23-19 just southwest of tank SX-115 (Fig. 4) are anomalous. These data are assumed to be a small fraction of total inventory in a known leak from tank SX-115 that was driven to the unconfined aquifer by a subsequent undetected leak in a water line located at the southwestern edge of the SX tank farm. Waterline leaks were not part of modeling in this study. While the magnitude and duration of the waterline leak cannot be quantified, local surface vegetation that persisted for several years, as well as uncharacteristically high moisture content in vadose zone sediments sampled from well 299-W23-19 (Fig. 4), suggests several years of leakage.

Similar conditions are not indicated near tank SX-108, where comparable maximum technetium-99 concentrations and technetium-99/(nitrate + nitrite) ratios are lower (e.g., about 8000 pCi $L^{-1}$ and 0.006 pCi $\mu g^{-1}$) at nearby downgradient well 299-W22-39 (Fig. 4). There is little evidence to suggest that the bulk of the contamination from the SX-108 tank leak has yet reached groundwater.

## Conclusions

The major observations and remarks, based on the numerical modeling, are as follows.

- Recharge estimates have a major influence on technetium-99 peak concentrations and their arrival times. No SX tank farm–specific recharge estimates are available. The base case infiltration rate of 100 mm $yr^{-1}$ was based on lysimeter data for gravel-covered, nonvegetated surfaces that mimic tank farm conditions.
- The fine-textured Cold Creek unit, with its higher moisture-holding capacity, can delay migration of contaminants to the water table. Following the initial rapid influx from tank leak, slow migration under natural recharge allowed the mobile species to migrate through the Hanford sands and reach the contact between the Hanford sands and the Cold Creek. The numerical results suggest that, while the Cold Creek unit can prolong the vadose zone residence time, the mobile contaminants do eventually break through the unit.
- Cesium-137 actively sorbs on to Hanford sediments; the cations show an apparent ion exchange front. The development of the ion exchange front, on the basis of the borehole data, can be used to postulate that the contaminant plume is more likely traveling through the far-field vadose zone sediments via porous media flow as opposed to traveling through preferred pathways. If the latter flow conditions were controlling the plume movement at the SX tank farm, it would be unlikely to encounter the well-developed ion exchange front throughout the borehole profile.
- The interim surface barriers, as expected, reduce fluxes to the water table. The technetium-99 peak concentration is reduced by more than a factor of six with placement of barriers but still exceedingly high. The two-dimensional modeling used in this study does not account for the additional mixing present in the third dimension; the predicted concentrations are therefore somewhat conservative.
- Simulated peak technetium-99 concentrations are considerably higher than those measured by the groundwater monitoring wells that are closest and east of the modeled cross-section, suggesting that the bulk of the contamination still resides within the vadose zone. The measured technetium-99 concentrations for well 299-W23-19 directly southwest of tank SX-115 have shown a persistent upward trend, but the contamination near SX-115 is unrelated to the leak from tank SX-108. Both groundwater monitoring data as well as numerical simulations show that cesium-137 does not reach the water table. The technetium-99 inventory is a small fraction of the cesium-137 inventory. However, because of its mobility and longevity, technetium-99 reaches groundwater at high concentrations.

### Acknowledgments

The work reported was performed for the U.S. Department of Energy Office of River Protection under Contract DE-AC06-99RL14047 with CH2M HILL Hanford Group, Inc. Suggestions provided by Glendon Gee (Pacific Northwest National Laboratory), Todd Rasmussen (University of Georgia), and an anonymous reviewer are greatly appreciated. Reference herein to any specific commercial product, process, or service by trade name, trademark, manufacturer, or otherwise does not necessarily constitute or imply its endorsement, recommendation, or favoring by the United States Government or any agency thereof or its contractors or subcontractors. The views and opinions of the authors do not necessarily state or reflect those of the United States Government or any agency thereof.

## References

Gardner, W.R. 1958. Some steady-state solutions of the unsaturated moisture flow equation with applications to evaporation from a water table. Soil Sci. 85:228–232.

Gee, G.W., M.J. Fayer, M.L. Rockhold, and M.D. Campbell. 1992. Variations in recharge at the Hanford Site. Northwest Sci. 66:237–250.

Gelhar, L.W. 1993. Stochastic subsurface hydrology. Prentice Hall, New York.

Gelhar, L.W., and C.L. Axness. 1983. Three-dimensional analysis of macrodispersion in a stratified aquifer. Water Resour. Res. 19:161–180.

Goodman, D. 2000. Estimation of SX-farm vadose zone Cs-137 inventories from geostatistical analysis of drywell and soil core data. HNF-5782, Rev. 0. Montana State Univ., Bozeman.

Hanlon, B.M. 2001. Waste tank summary report for month ending March 31, 2001. HNF-EP-0182, Rev. 156. CH2M HILL Hanford Group, Richland, WA.

Johnson, V.G., T.E. Jones, S.P. Reidel, and M.I. Wood. 1999. Subsurface physical conditions description of the S-SX waste management area. HNF-4936, Rev. 0. Fluor Daniel Hanford, Richland, WA.

Jones, T.E., R.A. Watrous, and G.T. MacLean. 2000. Inventory estimates for single-shell tank leaks in S and SX tank farms. RPP-6285, Rev. 0. CH2M HILL Hanford Group, Richland, WA.

Kaplan, D.L., and R.J. Serne. 1999. Geochemical data package for the immobilized low-activity waste performance assessment. PNNL-13037. Pacific Northwest National Laboratory, Richland, WA.

Khaleel, R., and E.J. Freeman. 1995. Variability and scaling of hydraulic properties for 200 Area soils, Hanford Site. WHC-EP-0883. Available at http://www.osti.gov/bridge/servlets/purl/188564-WXbGAs/webviewable/188564.pdf (verified 29 May 2007). Westinghouse Hanford Co., Richland, WA.

Khaleel, R., T.E. Jones, A.J. Knepp, F.M. Mann, D.A. Myers, P.M. Rogers, R.J. Serne, and M.I. Wood. 2000. Modeling data package for S-SX field investigation report (FIR). RPP-6296, Rev. 0. CH2M HILL Hanford Group, Richland, WA.

Khaleel, R., and J.F. Relyea. 1997. Correcting laboratory-measured moisture retention data for gravels. Water Resour. Res. 33:1875–1878.

Khaleel, R., J.F. Relyea, and J.L. Conca. 1995. Evaluation of van Genuchten–Mualem relationships to estimate unsaturated conductivity at low water contents. Water Resour. Res. 31:2659–2668.

Kline, N.W., and R. Khaleel. 1995. Effect of moisture-dependent anisotropy and enhanced recharge around underground storage tanks. WHC-SA-2680-FP. Westinghouse Hanford Co., Richland, WA.

Knepp, A.J. 2002. Field investigation report for waste management area S-SX. RPP-7884, Rev. 0. CH2M HILL Hanford Group, Richland, WA.

Lichtner, P.C., S. Yabusaki, K. Pruess, and C.I. Steefel. 2004. Role of competitive cation exchange on chromatographic displacement of cesium in the vadose zone beneath the Hanford S/SX tank farm. Vadose Zone J. 3:203–219.

Liu, C., J.M. Zachara, S.C. Smith, J.P. McKinley, and C.C. Ainsworth. 2003. Desorption kinetics of radiocesium from subsurface sediments at Hanford Site, USA. Geochim. Cosmochim. Acta 67:2893–2912.

McKinley, J.P., S.M. Heald, J.M. Zachara, M. Newville, and S. Sutton. 2004. Microscale distribution of cesium sorbed to biotite and muscovite. Environ. Sci. Technol. 38:1017–1023.

Millington, R.J., and J.P. Quirk. 1961. Permeability of porous solids. Trans. Faraday Soc. 57:1200–1207.

Mualem, Y. 1976. A new model for predicting the hydraulic conductivity of unsaturated porous media. Water Resour. Res. 12:513–522.

Myers, D.A., D.L. Parker, G. Gee, V.G. Johnson, G.V. Last, R.J. Serne, and D.J. Moak. 1998. Findings of the extension of borehole 41-09-39, 241-SX tank farm. HNF-2855. Lockheed Martin Hanford Corporation, Richland, WA.

Myers, D.A. 2001. Moisture distribution in the SX tank farm. RPP-7613, Rev. 0. CH2M HILL Hanford Group, Richland, WA.

Polmann, D.J. 1990. Application of stochastic methods to transient flow and transport in heterogeneous unsaturated soils. Ph.D. diss. Massachusetts Institute of Technology, Cambridge, MA.

Price, W.H., and K.R. Fecht. 1976. Geology of the 241-SX tank farm. ARH-LD-134. Atlantic Richfield Hanford Co., Richland, WA.

Pruess, K., S. Yabusaki, C. Steefel, and P. Lichtner. 2002. Fluid flow, heat transfer, and solute transport at nuclear waste storage tanks in the Hanford vadose zone. Vadose Zone J. 1:68–88.

Raymond, J.R., and E.G. Shdo. 1966. Characterization of subsurface contamination in the SX tank farm. BNWL-CC-701. Battelle Northwest Laboratory, Richland, WA.

Serne, R.J., G.V. Last, G.W. Gee, H.T. Schaef, D.C. Lanigan, C.W. Lindenmeier, R.E. Clayton, V.L. LeGore, R.D. Orr, M.J. O'Hara, C.F. Brown, D.B. Burke, A.T. Owen, I.V. Kutnyakov, T.C. Wilson, and D.A. Myers. 2001a. Geologic and geochemical data collected from vadose zone sediments from borehole SX 41-09-39 in the S/SX waste management area and preliminary interpretations. PNNL-2001-2. Pacific Northwest National Laboratory, Richland, WA.

Serne, R.J., H.T. Schaef, G.V. Last, D.C. Lanigan, C.W. Lindenmeier, C.C. Ainsworth, R.E. Clayton, V.L. LeGore, M.J. O'Hara, C.F. Brown, R.D. Orr, I.V. Kutnyakov, T.C. Wilson, K.B. Wagnon, B.A. Williams, and D.B. Burke. 2001b. Geologic and geochemical data collected from vadose zone sediments from slant borehole [SX-108] in the S/SX waste management area and preliminary interpretations. PNNL-2001-4. Pacific Northwest National Laboratory, Richland, WA.

Sisson, J.B., and A.H. Lu. 1984. Field calibration of computer models for application to buried liquid discharges: A status report. RHO-ST-46P. Rockwell Hanford Operations, Richland, WA.

Steefel, C.I., S. Carroll, P.H. Zhao, and S. Roberts. 2003. Cesium migration in Hanford sediment: A multisite cation exchange model based on laboratory transport experiments. J. Contam. Hydrol. 67:219–246.

Talbott, M.E., and L.W. Gelhar. 1994. Performance assessment of a hypothetical low-level waste facility: Groundwater flow and transport simulation. NUREG/CR-6114. Vol. 3. U.S. Nuclear Regulatory Commission, Washington, DC.

van Genuchten, M.Th. 1980. A closed-form equation for predicting the hydraulic conductivity of unsaturated soils. Soil Sci. Soc. Am. J. 44:892–898.

Ward, A.L., T.G. Caldwell, and G.W. Gee. 2000. Vadose zone transport field study: Soil water content distributions by neutron moderation. PNNL-13795. Available at http://vadose.pnl.gov/files/13795.pdf (verified 29 May 2007). Pacific Northwest National Laboratory, Richland, WA.

Ward, A.L., G.W. Gee, and M.D. White. 1997. A comprehensive analysis of contaminant transport in the vadose zone beneath tank SX-109. PNNL-11463. Pacific Northwest National Laboratory, Richland, WA. Available at http://www.osti.gov/bridge/servlets/purl/475663-qOZpCu/webviewable/475663.pdf (verified 29 May 2007).

Ward, A.L., Z.F. Zhang, and G.W. Gee. 2006. Upscaling unsaturated hydraulic parameters for flow through heterogeneous, anisotropic sediments. Adv. Water Resour. 29(2):268–280.

White, M.D., and M. Oostrom. 2000a. STOMP subsurface transport over multiple phases, version 2.0, theory guide. PNNL-12030, UC-2010. Pacific Northwest National Laboratory, Richland, WA.

White, M.D., and M. Oostrom. 2000b. STOMP subsurface transport over multiple phases, version 2.0, user's guide. PNNL-12034, UC-2010. Pacific Northwest National Laboratory, Richland, WA.

White, M.D., M. Oostrom, and M.D. Williams. 2001. FY00 initial assessment for S-SX field investigation report (FIR): Simulations of contaminant migration and surface barriers. PNWD-3111. Battelle, Pacific Northwest Division, Richland, WA.

White, M.D., S.B. Yabusaki, and K. Pruess. 2002. Nonisothermal multiphase fluid flow and transport: Multitank modeling in the SX tank farm. p. D-277–D-305. *In* A.J. Knepp (ed.) Field investigation report for waste management area S-SX. RPP-7884, Rev. 0. CH2M HILL Hanford Group, Richland, WA.

Ye, M., R. Khaleel, and T.-C.J. Yeh. 2005. Stochastic analysis of moisture plume dynamics of a field injection experiment. Water Resour. Res. 41:W03013, doi:10.1029/2004WR003735.

Yeh, T.-C., L.W. Gelhar, and A.L. Gutjahr. 1985. Stochastic analysis of unsaturated flow in heterogeneous soils: 2. Statistically anisotropic media with variable $\alpha$. Water Resour. Res. 21:457–464.

Yeh, T.-C.J., M. Ye, and R. Khaleel. 2005. Estimation of effective unsaturated hydraulic conductivity tensor using spatial moments of observed moisture plume. Water Resour. Res. 41:W03014, doi:10.1029/2004WR003736.

Zachara, J.M., S.C. Smith, C. Liu, J.P. McKinley, R.J. Serne, and P.L. Gassman. 2002. Sorption of $Cs^+$ to micaceous subsurface sediments from the Hanford Site, USA. Geochim. Cosmochim. Acta 66:193–211.